



Is the Black-widow Pulsar PSR J1555–2908 in a Hierarchical Triple System?

L. Nieder^{1,2} , M. Kerr³ , C. J. Clark^{1,2,4} , P. Bruel⁵ , H. T. Cromartie^{6,8} , S. M. Ransom⁷ , and P. S. Ray³ ¹Max-Planck-Institut für Gravitationsphysik (Albert-Einstein-Institut), D-30167 Hannover, Germany; lars.nieder@aei.mpg.de²Leibniz Universität Hannover, D-30167 Hannover, Germany³Space Science Division, Naval Research Laboratory, Washington, DC 20375-5352, USA⁴Jodrell Bank Centre for Astrophysics, Department of Physics and Astronomy, The University of Manchester, Manchester M13 9PL, UK⁵Laboratoire Leprince-Ringuet, CNRS, École polytechnique, Institut Polytechnique de Paris, F-91120 Palaiseau, France⁶Cornell Center for Astrophysics and Planetary Science, and Department of Astronomy, Cornell University, Ithaca, NY 14853, USA⁷National Radio Astronomy Observatory, 520 Edgemont Road, Charlottesville, VA 22903, USA

Received 2022 February 10; revised 2022 April 27; accepted 2022 April 28; published 2022 May 18

Abstract

The 559 Hz black-widow pulsar PSR J1555–2908, originally discovered in radio, is also a bright gamma-ray pulsar. Timing its pulsations using 12 yr of Fermi-Large Area Telescope gamma-ray data reveals long-term variations in its spin frequency that are much larger than is observed from other millisecond pulsars. While this variability in the pulsar rotation rate could be intrinsic “timing noise,” here we consider an alternative explanation: the variations arise from the presence of a very-low-mass third object in a wide multiyear orbit around the neutron star and its low-mass companion. With current data, this hierarchical-triple-system model describes the pulsar’s rotation slightly more accurately than the best-fitting timing noise model. Future observations will show if this alternative explanation is correct.

Unified Astronomy Thesaurus concepts: [Gamma-ray sources \(633\)](#); [Millisecond pulsars \(1062\)](#); [Pulsar planets \(1304\)](#); [Pulsar timing method \(1305\)](#)

1. Introduction

PSR J1555–2908, a neutron star spinning rapidly at 559 Hz, resides in a tight 5.5 hr binary system (Ray et al. 2022, hereafter Paper I) with a low-mass ($0.06 M_{\odot}$) companion (Kennedy et al. 2022). This millisecond pulsar (MSP) was first detected in a Green Bank Telescope (GBT) pulsar survey that targeted steep-spectrum radio sources (Frail et al. 2018) within the localization region of Fermi-Large Area Telescope (LAT; Atwood et al. 2009) gamma-ray sources. After the radio discovery, gamma-ray pulsations were detected, allowing the timing measurement of the system parameters over the 12 yr Fermi mission time span.

Timing analysis using the LAT data reveals variations of the spin frequency f that are larger than is typical for MSPs (Kerr et al. 2015). Such variations are often seen in young gamma-ray pulsars, where they are labeled as “timing noise.” Timing noise is also present in MSPs, but its weaker amplitude (Shannon & Cordes 2010) is typically not detectable with the LAT (Ajello et al. 2022). Instead, the intrinsic rotational phase is generally well described by a quadratic function of time, i.e., a constant spin-down rate \dot{f} , with no detectable noise components above the measurement uncertainty. In contrast, for PSR J1555–2908 four additional terms in the rotational phase model are required.⁹

⁸ NASA Hubble Fellowship Program Einstein Postdoctoral Fellow.

⁹ In a gamma-ray timing analysis, this is easily distinctive from the variations of the orbital period that are often seen in “spider” pulsars. While both variations happen on multiyear timescales, spin-frequency variations manifest as pulse phase drift, and variations of the short ($\lesssim 1$ day) orbital period smear the pulse profile out.

Such strong variations suggest an alternative explanation. For example, in the case of the millisecond pulsar PSR J1024–0719, long thought to be isolated, the measurement of additional higher-order spin-frequency derivatives led to the conclusion that the pulsar could be in a very-long-period (> 2 kyr) orbit with a low-mass companion (Kaplan et al. 2016).

In this Letter, we discuss a similar alternative to the timing noise explanation for PSR J1555–2908: the variations arise from the presence of a third body in the system. This additional object is in a wide, multiyear orbit around the closely orbiting neutron star and its low-mass companion. An extreme example of such a system would be the hierarchical-triple-system (HTS) pulsar PSR J0337+1715 (Ransom et al. 2014).

With the currently available data, this model describes the pulsar as well as the timing noise model, but provides a simple and clear physical explanation for the spin-frequency variations.

2. Rotational Phase Model

To precisely track the rotational phase, the photon arrival times need to be corrected for the line-of-sight motion of the pulsar, if it is in an orbit with one or more companions. For a simple HTS, we assume that the gravitational interaction between the two companions can be neglected, and the third body orbits the center of mass of the inner binary system. The photon times, corrected for the pulsar’s motion around the barycenter of the triple system, t_{tb} , can be expressed as a function of the photon’s emission time, t_{em} , as

$$t_{\text{tb}} = t_{\text{em}} + x_i \Delta_i(\Omega_i t_{\text{em}}) + x_o \Delta_o(\Omega_o t_{\text{em}}). \quad (1)$$

Here, x_i and x_o are the times light needs to travel the semimajor axis of the pulsar’s orbit due to the inner (i) and outer (o) companion projected onto the line of sight. Δ_i and Δ_o are dimensionless functions that describe the respective modulations depending on the orbital phases, $\Omega_i t_{\text{em}}$ and $\Omega_o t_{\text{em}}$. The

orbital angular frequencies Ω_i and Ω_o are defined by the orbital periods P_i and P_o via $\Omega_i = 2\pi/P_i$ and $\Omega_o = 2\pi/P_o$.

Following Edwards et al. (2006), we can make $x_i\Delta_i(\Omega_i t_{em}) + x_o\Delta_o(\Omega_o t_{em})$ a function of t_{tb} by Taylor expansion. To second order (i.e., including terms of order $(x_i\Omega_i)^2$, $(x_o\Omega_o)^2$, $x_ix_o\Omega_i^2$, and $x_ix_o\Omega_o^2$), we find

$$\begin{aligned} & x_i\Delta_i(\Omega_i t_{em}) + x_o\Delta_o(\Omega_o t_{em}) \\ & \approx (x_i\Delta_i(\Omega_i t_{tb}) + x_o\Delta_o(\Omega_o t_{tb})) \\ & \times [1 - (x_i\Omega_i\Delta_i'(\Omega_i t_{tb}) + x_o\Omega_o\Delta_o'(\Omega_o t_{tb})) \\ & + (x_i\Omega_i\Delta_i'(\Omega_i t_{tb}) + x_o\Omega_o\Delta_o'(\Omega_o t_{tb}))^2 \\ & + \frac{1}{2}(x_i\Omega_i^2\Delta_i''(\Omega_i t_{tb}) + x_o\Omega_o^2\Delta_o''(\Omega_o t_{tb})) \\ & \times (x_i\Delta_i(\Omega_i t_{tb}) + x_o\Delta_o(\Omega_o t_{tb}))], \end{aligned} \quad (2)$$

where Δ' and Δ'' denote the first and second derivative of Δ with respect to Ωt . For wide, multiyear outer orbits of low-mass companions, $x_o\Omega_o \ll x_i\Omega_i$, so we neglect terms multiplied by this quantity, i.e., $\Delta_o' = 0$ and $\Delta_o'' = 0$.

In the case of a circular orbit, Δ takes the simple form of a sinusoid, $\Delta(t) = \sin(\Omega(t - T_{asc}))$, with time of ascending node T_{asc} . Hence, $\Delta'(t) = \cos(\Omega(t - T_{asc}))$ and $\Delta''(t) = -\sin(\Omega(t - T_{asc}))$. Equation (2) can also be applied to the widely used small-eccentricity-orbit ‘‘ELL1 model’’ (Lange et al. 2001), or the larger-eccentricity models presented in Nieder et al. (2020).

For the outer companion’s orbit of PSR J1555–2908, we use the full ‘‘BT model,’’ $\Delta(t) = \sin\omega(\cos E - e) + \sqrt{1 - e^2} \cos\omega \sin E$ with eccentricity e , and angle of periastron ω (Blandford & Teukolsky 1976). E is defined via $E - e \sin E = \Omega(t - T_0)$ and is computed numerically. Instead of using the parameter set $\{T_0, e, \omega\}$, which is degenerate for small eccentricities, we use $T_{asc} = T_0 - \omega/\Omega$, $\epsilon_1 = e \sin\omega$, and $\epsilon_2 = e \cos\omega$ (Lange et al. 2001).

In Section 3, we show that PSR J1555–2908 can be well described as an HTS with the inner orbit being circular and the outer orbit being eccentric.

For a timing analysis, it is helpful to have a good starting point in the multidimensional parameter space. The parameters describing the potential outer orbit can be roughly estimated from the timing solution presented in Paper I, which requires four additional frequency derivatives (‘‘FX model’’).

First, we need to derive how the observed frequency changes in the case of an outer circular orbit. Assuming only a nonzero spin frequency f and a nonzero first time-derivative \dot{f} , the additional evolution of the spin frequency over time can be written in two ways:

$$\begin{aligned} & f(t) - f_* - \dot{f}_*(t - t_0) \\ & = \frac{1}{2}f_*^{(2)}(t - t_0)^2 + \frac{1}{6}f_*^{(3)}(t - t_0)^3 \\ & + \frac{1}{24}f_*^{(4)}(t - t_0)^4 \\ & + \frac{1}{120}f_*^{(5)}(t - t_0)^5 \\ & = \Delta f_* + \Delta \dot{f}_*(t - t_0) \\ & - (f_* + \Delta f_*)x_o\Omega_o \cos(\Omega_o(t - T_{asc,o})). \end{aligned} \quad (3)$$

Here, we denote the n th frequency derivative as $f^{(n)}$, and use an asterisk to indicate parameters measured with the FX model, and $\Delta f_* = f - f_*$ as well as $\Delta \dot{f}_* = \dot{f} - \dot{f}_*$. t_0 denotes the chosen reference time.

Second, since all parameters in Equation (3) are measured, we fit Equation (4) to Equation (3) over the valid time span of the pulsar timing solution. To do this, we used `curve_fit` from `scipy`. This gives initial values for the five free parameters $\{\Delta f_*, \Delta \dot{f}_*, x_o, \Omega_o, T_{asc,o}\}$ from Equation (4).

From the fitted values, we find the inner binary barycenter’s potential movement would have a radius of a few tens of kilometers with an orbital period of ~ 10 yr, indicating a low-mass companion in a wide orbit.

This approach can be compared with the outer-orbital-parameter estimation method presented by Joshi & Rasio (1997), who worked with a similar number of spin-frequency derivatives. Joshi & Rasio (1997) equate the observed spin-frequency derivatives, measured over a small fraction of an orbital period, to the first terms in the Taylor series expansion of the outer orbit’s sinusoidal modulation, and solve analytically for the orbital parameters. This method works for a sufficiently large modulation amplitude and high-precision determination of the frequency derivatives via radio timing. For PSR J1555–2908, only five frequency derivatives are measurable in the gamma-ray data covering roughly one orbit, which may be interpreted as globally best-fitting values that describe the modulation over the full data set, rather than instantaneous measurements of the derivatives of the orbital sinusoid. Because the data span is similar to the outer-orbital period, the fitting method presented in this work also provides an estimate of \dot{f} , which must be known or guessed in the method of Joshi & Rasio (1997).

3. Gamma-Ray Timing Analysis

In our timing analysis, we use the LAT data prepared for the timing in Paper I. These data include P8R3 SOURCE-class photons (Atwood et al. 2013; Bruel et al. 2018) detected by LAT between 2008 August 3 and 2020 August 5 within a 5° region of interest around the pulsar position, with energies greater than 100 MeV, and with a maximum zenith angle of 90° .

The timing analysis is done twice, very similarly to the approach in Paper I. First, we refit all the parameters of the FX model, i.e., we did not fix any parameters to the radio timing solution. Second, we amended the timing code with the HTS model given in Equations (1) and (2). To judge the timing results, we used the H statistic (de Jager et al. 1989; Kerr 2011) with the photon probability weights optimized following Bruel (2019), the likelihood \mathcal{L} (Abdo et al. 2013), and the Bayesian information criterion (BIC; Schwarz 1978). The latter is based on the likelihood but with a penalty factor proportional to the degrees of freedom to penalize higher-dimensional models.

In the timing analysis, we tried to find the parameters that maximize \mathcal{L} for a given model (see, e.g., Clark et al. 2017). \mathcal{L} represents the likelihood that the pulse profile, i.e., the distribution of the pulsar’s phases at the emission time of the LAT-detected photons, is described by a given pulse template. Here, the pulsar phases are computed using either the FX or the HTS model, with the associated parameters. To explore the parameter space, we use a Monte Carlo sampling algorithm

Table 1
Timing Solutions for PSR J1555–2908 with FX and HTS Models

Parameter	FX Value	HTS Value
Range of observational data (MJD)	54681–59066	
Reference epoch (MJD)	57800.0	
Statistics		
H statistic	908.7	940.2
Log-Likelihood $\log \mathcal{L}$	283.7	288.1
BIC	–444.9	–446.5
Timing parameters		
R.A., α (J2000.0)	15 ^h 55 ^m 40 ^s .6587(2)	15 ^h 55 ^m 40 ^s .6586(2)
Decl., δ (J2000.0)	–29°08′28″.424(8)	–29°08′28″.424(7)
Spin frequency, f (Hz)	559.44000642607(5)	559.44000642558(17)
1st spin-frequency derivative, \dot{f} (Hz s ^{–1})	–1.39361(18) $\times 10^{-14}$	–1.39232(12) $\times 10^{-14}$
2nd spin-frequency derivative, $f^{(2)}$ (Hz s ^{–2})	5.6(4) $\times 10^{-25}$	
3rd spin-frequency derivative, $f^{(3)}$ (Hz s ^{–3})	1(2) $\times 10^{-33}$	
4th spin-frequency derivative, $f^{(4)}$ (Hz s ^{–4})	–2.0(6) $\times 10^{-40}$	
5th spin-frequency derivative, $f^{(5)}$ (Hz s ^{–5})	–3.4(8) $\times 10^{-48}$	
Inner-orbit binary parameters		
Proj. semimajor axis, x_i (lt-s)	0.151445(3)	0.151444(3)
Orbital period, P_i (days)	0.23350026827(13)	0.23350026831(12)
Epoch of ascending node, $T_{\text{asc},i}$ (MJD)	57785.5393610(8)	57785.5393612(8)
Outer-orbit binary parameters		
Proj. semimajor axis, x_o (lt-s)		0.000155(20)
Orbital period, P_o (days)		4.5(4) $\times 10^3$
Epoch of ascending node, $T_{\text{asc},o}$ (MJD)		54840(140)
1st Laplace-Lagrange parameter, $\epsilon_{1,o}$		0.27(5)
2nd Laplace-Lagrange parameter, $\epsilon_{2,o}$		0.02(7)

Note. Numbers in parentheses are statistical 1σ uncertainties on the final digits. The JPL DE405 solar system ephemeris has been used, and times refer to TDB.

(Goodman & Weare 2010), following the efficient parallelization scheme from Foreman-Mackey et al. (2013).

In the case of the HTS model, we tested the circular and eccentric options, where the latter requires two additional parameters. The eccentric orbit model is favored by all three statistics. For the FX model, we added spin-frequency derivatives until the test statistics H and \mathcal{L} stopped improving significantly, which is in turn disfavored by the BIC. Here, adding six additional derivatives in principle leads to H and \mathcal{L} values of a similar size to the HTS model. However, the last model favored by the BIC is the one with four additional frequency derivatives. The final timing solutions for the FX and HTS models are reported in Table 1.

In the timing analysis with the HTS model, the highest test statistics are found for an eccentric ($e_o \sim 0.27$) outer orbit of ~ 4500 days. With the LAT data span being only slightly shorter, the spin parameters f and \dot{f} are still correlated with the outer-orbit Keplerian parameters P_o , x_o , and $T_{\text{asc},o}$. However, this covariance is small enough to not pose a problem for the timing analysis. Note, that the timing analysis does not give any information on the inclination between the orbits as only the line-of-sight motion can be measured.

The highest test statistics, H and \mathcal{L} , seem to favor the HTS model over the FX model (see Table 1). Since each model has a different number of free parameters, we invoke the BIC. The BIC’s penalty for the additional parameter removes most of the advantage the HTS model had. However, the BIC still slightly favors the HTS model over the FX model ($\Delta\text{BIC} = -1.6$). Our

final timing solutions over 12 yr of LAT data using the FX model and the HTS model are shown in Table 1.

In order to more directly compare the timing noise to that of other MSPs, we have analyzed it by following the methods of Lentati et al. (2014), adapted to gamma-ray data as in Ajello et al. (2022). In this approach, the timing noise is assumed to originate in a stationary process, thus having a unique description with a power spectral density that we assume follows a power law, $P(f) = P_{\text{tn}}(f \times \text{yr})^{-\Gamma_{\text{tn}}}$. The timing model parameters, the timing noise parameters Γ and P_{tn} , and the Fourier coefficients of the timing noise process are all determined jointly by maximizing the likelihood, which includes a Gaussian component that constrains the Fourier coefficients to follow the specified power law. We estimate uncertainties on the timing noise parameters from the curvature of the likelihood at its maximum value, and obtain $\log_{10}(P_{\text{tn}} \times \text{s}^{-2} \text{yr}) = -13.3 \pm 1.3$ and spectral index $\Gamma_{\text{tn}} = 6.0 \pm 1.4$.

4. Discussion

The spin-frequency variations of PSR J1555–2908 (see also Paper I) are unusually large in amplitude for the timing noise of an MSP (Kerr et al. 2015). Indeed, Figure 1 shows the timing noise spectral properties for two samples of MSPs as measured by the pulsar timing arrays (PTAs) NANOGrav (Arzoumanian et al. 2020; Alam et al. 2021) and the PPTA (Goncharov et al. 2021), along with our measured values for PSR J1555–2908. It is possible this collection of timing noise measurements is

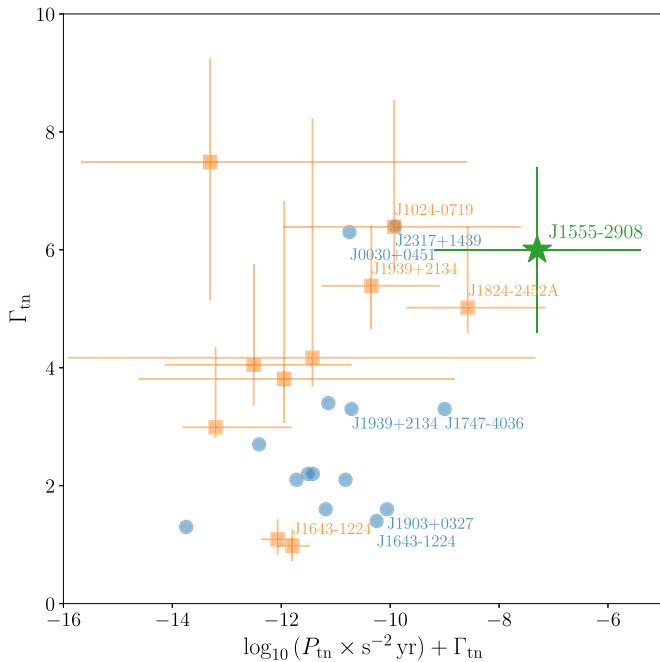


Figure 1. Measured values of the timing noise power P_{tn} and spectral index Γ_{tn} from NANOGrav (blue circles) and the PPTA (orange squares). 1σ uncertainties for the PPTA pulsars are taken from Table 1 by Goncharov et al. (2021). The addition of Γ_{tn} to the abscissa converts the power normalization from a frequency of $f = 1 \text{ yr}^{-1}$ to $f = 0.1 \text{ yr}^{-1}$. The measured value for PSR J1555–2908 (this work) is depicted with a green star. Pulsars with strong timing noise are labeled.

biased by selection for inclusion in a PTA. However, the driving concern for inclusion is radio brightness, and often timing noise emerges only after many years of observation. Consequently, we expect such a bias to be modest. The abscissa in Figure 1 is defined in such a way to indicate the timing noise at frequency $f = 0.1 \text{ yr}^{-1}$, i.e., a timescale comparable to the length of the data set. PSR J1555–2908 is a clear outlier, with more than 10 times the timing noise amplitude of the next strongest pulsar, PSR J1824–2452A in the M28 globular cluster, whose timing noise presumably includes contributions from the cluster potential and close passages by other cluster members. Another noteworthy example is PSR J1939+2134, an isolated MSP considered to be a “noisy” timer for which Shannon et al. (2013) invoked an asteroid belt surrounding the pulsar to explain the observed timing variations, but which has a timing noise amplitude that is 1000 times weaker than that of PSR J1555–2908.

In this work we have presented an alternative explanation, in which another companion orbits the inner binary system, an HTS. To account for the additional body in the system, we have developed a simple, but sufficient rotational phase model. In a timing analysis with current data, the results with both models are indistinguishable. Within the timing range the maximum phase offset between both models is $< 1\%$ of one rotation.

It is predictable that the two models would not differ much. The variations are measurable with the LAT data, but the peak-to-peak amplitude of the phase offset is still only 17% of one rotation. Furthermore, the potential outer companion would have completed roughly one orbit during the Fermi mission, which can be well approximated with the six spin parameters of the FX model.

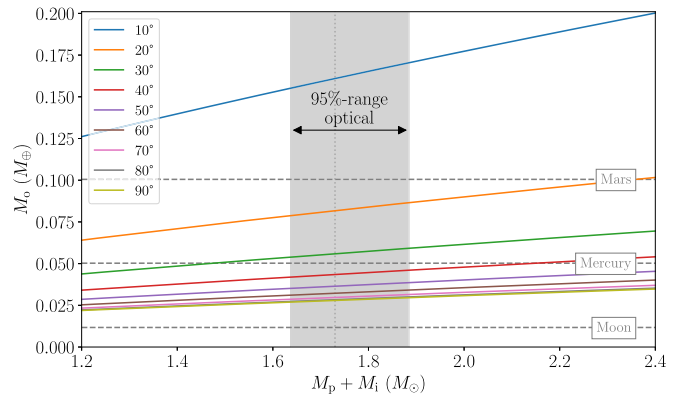


Figure 2. Mass–mass diagram where lines show the potential outer companion mass for different inclination angles (measured with respect to line of sight to Earth) and total masses of the inner binary system. For comparison, the masses of the Moon, Mercury, and Mars are indicated by the dashed lines. The dotted line and the gray area mark the most likely value for $M_p + M_i = 1.73 M_\odot$ and the associated 95% range from optical modeling (Kennedy et al. 2022).

In the following, we will make estimates of the companion mass and the orbital radius, but want to note that these directly depend on the outer orbital period P_o . Due to the strong correlations between the orbital parameters (see Section 3), these estimates should be treated with caution and will only give an order of magnitude.

The binary mass function may be used to estimate the mass of the outer companion (see Figure 2). For common pulsar masses $1.4 M_\odot < M_p < 2.0 M_\odot$, an inner companion mass $M_i = 0.06 M_\odot$ (Kennedy et al. 2022), and inclination angles 30° – 90° , the outer companion would have roughly a Mercury-like mass $0.02 M_\oplus \lesssim M_o \lesssim 0.06 M_\oplus$. To date, this companion would still be listed among the four lowest-mass extrasolar planets.¹⁰

A comparably low-mass ($\sim 0.015 M_\oplus$) companion has also been found for a planet orbiting PSR B1257+12 (Wolszczan 1994), the pulsar thanks to which, 30 yr ago, the first extrasolar planetary companions have been identified (Wolszczan & Frail 1992). However, unlike the periods of the planets orbiting PSR B1257+12 with tens to hundreds of days, the probable companion of PSR J1555–2908 takes considerably longer with $P_o \sim 4500$ days.

The putative triple system of PSR J1555–2908 is extremely hierarchical. The pulsar’s mass is ~ 28 times larger than the inner companion’s mass, and even $\sim 10^7$ times larger than the outer companion’s mass. The ratio between outer and inner orbital period is $P_o/P_i \approx 20,000$. Using Kepler’s third equation, the masses from optical modeling, and the timing parameters one can estimate the semimajor axis of the inner companion’s orbit as $\sim 4.2 \text{ lt-s}$ and the outer companion’s orbit as $\sim 3200 \text{ lt-s}$. Systems with such extreme hierarchical properties are typically assumed to be stable on long timescales (Georgakarakos 2008).

Other HTSs that include a pulsar are known. PSR J0337+1715 is in an orbit with two white dwarf companions (Ransom et al. 2014). Carefully studying this system led to one of the most stringent tests of general relativity’s predicted universality of freefall (Archibald et al. 2018; Voisin et al. 2020). A binary system consisting of the MSP PSR B1620–20

¹⁰ <http://exoplanet.eu/catalog/>

and a white dwarf is orbited by a planetary companion of $\sim 2.5 M_{\text{Jupiter}}$ (Thorsett et al. 1993; Sigurdsson et al. 2003).

An open question is how such a system could have formed. A pulsar planet can form in various ways (see, e.g., Podsiadlowski 1993). Since PSR J1555–2908 is not in a dense globular cluster, it seems unlikely that the triple was formed in an exchange interaction between systems as is suggested for PSR B1620–20 (Sigurdsson et al. 2003). Another option could be that the inner binary captured a free-floating planet (see, e.g., Miret-Roig et al. 2021). On the other hand, the planet might have formed from a circumbinary debris disk (see, e.g., Pelupessy & Portegies Zwart 2013), in which case it would be expected that the orbits are coplanar.

Only to emphasize the power of pulsar timing with LAT data, we want to note that if PSR J1555–2908 has an additional planetary-mass companion, then it was discovered because over the course of 100 billion pulsar rotations, the phase drifted by 17% of one single rotation. The higher precision of a radio timing campaign would provide more sensitivity to discriminate between an eccentric HTS model and stochastic timing noise, and would pin down the probable outer-orbit parameters more precisely in the long term than the presented gamma-ray timing analysis. However, this would require many years of regular radio observations before a qualitative improvement over gamma-ray timing alone would be realized.

So, is PSR J1555–2908 in a hierarchical triple system? We do not know, yet. With current data, both of the timing models that are presented here track the pulsar’s rotation equally well. However, the ongoing Fermi mission will continue to collect data, and eventually the nature of this system will be resolved.

We thank the anonymous referee for their valuable comments. This work was supported by the Max-Planck-Gesellschaft (MPG). C.J.C. acknowledges support from the ERC under the European Union’s Horizon 2020 research and innovation program (grant agreement No. 715051; Spiders). Portions of this work performed at NRL were supported by NASA. The National Radio Astronomy Observatory is a facility of the National Science Foundation operated under cooperative agreement by Associated Universities, Inc. S.M.R. is a CIFAR Fellow and is supported by the NSF Physics Frontiers Center awards 1430284 and 2020265. Support for H.T.C. is provided by NASA through the NASA Hubble Fellowship Program grant #HST-HF2-51453.001 awarded by the Space Telescope Science Institute, which is operated by the Association of Universities for Research in Astronomy, Inc., for NASA, under contract NAS5-26555.

The Fermi LAT Collaboration acknowledges generous ongoing support from a number of agencies and institutes that have supported both the development and the operation of the LAT as well as scientific data analysis. These include the National Aeronautics and Space Administration and the Department of Energy in the United States, the Commissariat à l’Energie Atomique and the Centre National de la Recherche Scientifique/Institut National de Physique Nucléaire et de Physique des Particules in France, the Agenzia Spaziale Italiana and the Istituto Nazionale di Fisica Nucleare in Italy, the Ministry of Education, Culture, Sports, Science and Technology (MEXT), High Energy Accelerator Research

Organization (KEK) and Japan Aerospace Exploration Agency (JAXA) in Japan, and the K. A. Wallenberg Foundation, the Swedish Research Council and the Swedish National Space Board in Sweden.

Additional support for science analysis during the operations phase is gratefully acknowledged from the Istituto Nazionale di Astrofisica in Italy and the Centre National d’Études Spatiales in France. This work performed in part under DOE Contract DE-AC02-76SF00515.

ORCID iDs

L. Nieder  <https://orcid.org/0000-0002-5775-8977>
 M. Kerr  <https://orcid.org/0000-0002-0893-4073>
 C. J. Clark  <https://orcid.org/0000-0003-4355-3572>
 P. Bruel  <https://orcid.org/0000-0002-9032-7941>
 H. T. Cromartie  <https://orcid.org/0000-0002-6039-692X>
 S. M. Ransom  <https://orcid.org/0000-0001-5799-9714>
 P. S. Ray  <https://orcid.org/0000-0002-5297-5278>

References

- Abdo, A. A., Ajello, M., Allafort, A., et al. 2013, *ApJS*, **208**, 17
 Ajello, M., Atwood, W. B., Baldini, L., et al. 2022, *Sci*, **376**, 521
 Alam, M. F., Arzoumanian, Z., Baker, P. T., et al. 2021, *ApJS*, **252**, 4
 Archibald, A. M., Gusinskaia, N. V., Hessels, J. W. T., et al. 2018, *Natur*, **559**, 73
 Arzoumanian, Z., Baker, P. T., Blumer, H., et al. 2020, *ApJL*, **905**, L34
 Atwood, W., Albert, A., Baldini, L., et al. 2013, arXiv:1303.3514
 Atwood, W. B., Abdo, A. A., Ackermann, M., et al. 2009, *ApJ*, **697**, 1071
 Blandford, R., & Teukolsky, S. A. 1976, *ApJ*, **205**, 580
 Bruel, P. 2019, *A&A*, **622**, A108
 Bruel, P., Burnett, T. H., Digel, S. W., et al. 2018, arXiv:1810.11394
 Clark, C. J., Wu, J., Pletsch, H. J., et al. 2017, *ApJ*, **834**, 106
 de Jager, O. C., Raubenheimer, B. C., & Swanepoel, J. W. H. 1989, *A&A*, **221**, 180
 Edwards, R. T., Hobbs, G. B., & Manchester, R. N. 2006, *MNRAS*, **372**, 1549
 Foreman-Mackey, D., Hogg, D. W., Lang, D., & Goodman, J. 2013, *PASP*, **125**, 306
 Frail, D. A., Ray, P. S., Mooley, K. P., et al. 2018, *MNRAS*, **475**, 942
 Georgakarakos, N. 2008, *CeMDA*, **100**, 151
 Goncharov, B., Reardon, D. J., Shannon, R. M., et al. 2021, *MNRAS*, **502**, 478
 Goodman, J., & Weare, J. 2010, *Commun. Appl. Math. Comput. Sci.*, **5**, 65
 Joshi, K. J., & Rasio, F. A. 1997, *ApJ*, **479**, 948
 Kaplan, D. L., Kupfer, T., Nice, D. J., et al. 2016, *ApJ*, **826**, 86
 Kennedy, M. R., Breton, R. P., Clark, C. J., et al. 2022, *MNRAS*, **512**, 3001
 Kerr, M. 2011, *ApJ*, **732**, 38
 Kerr, M., Ray, P. S., Johnston, S., Shannon, R. M., & Camilo, F. 2015, *ApJ*, **814**, 128
 Lange, C., Camilo, F., Wex, N., et al. 2001, *MNRAS*, **326**, 274
 Lentati, L., Alexander, P., Hobson, M. P., et al. 2014, *MNRAS*, **437**, 3004
 Miret-Roig, N., Bouy, H., Raymond, S. N., et al. 2021, *NatAs*, **6**, 89
 Nieder, L., Allen, B., Clark, C. J., & Pletsch, H. J. 2020, *ApJ*, **901**, 156
 Pelupessy, F. I., & Portegies Zwart, S. 2013, *MNRAS*, **429**, 895
 Podsiadlowski, P. 1993, in ASP Conf. Ser. 36, Planets Around Pulsars, ed. J. A. Phillips, S. E. Thorsett, & S. R. Kulkarni (San Francisco, CA: ASP), 149
 Ransom, S. M., Stairs, I. H., Archibald, A. M., et al. 2014, *Natur*, **505**, 520
 Ray, P. S., Nieder, L., Clark, C. J., et al. 2022, *ApJ*, **927**, 216
 Schwarz, G. 1978, *AnSta*, **6**, 461
 Shannon, R. M., & Cordes, J. M. 2010, *ApJ*, **725**, 1607
 Shannon, R. M., Cordes, J. M., Metcalfe, T. S., et al. 2013, *ApJ*, **766**, 5
 Sigurdsson, S., Richer, H. B., Hansen, B. M., Stairs, I. H., & Thorsett, S. E. 2003, *Sci*, **301**, 193
 Thorsett, S. E., Arzoumanian, Z., & Taylor, J. H. 1993, *ApJL*, **412**, L33
 Voisin, G., Cognard, I., Freire, P. C. C., et al. 2020, *A&A*, **638**, A24
 Wolszczan, A. 1994, *Sci*, **264**, 538
 Wolszczan, A., & Frail, D. A. 1992, *Natur*, **355**, 145